Journal of Molecular Structure 1048 (2013) 331–338

Contents lists available at SciVerse ScienceDirect

Journal of Molecular Structure

journal homepage: www.elsevier.com/locate/molstruc

A structural and vibrational study of dehydrofukinone combining FTIR, FTRaman, UV–visible and NMR spectroscopies with DFT calculations

Emilio Lizarraga [a], Elida Romano [b], Ana B. Raschi [b], Patricio Leyton [c], Carolina Paipa [d], César A.N. Catalán [a], Silvia A. Brandán [b,*]

[a] INQUINOA-CONICET, Instituto de Química Orgánica, Facultad de Bioquímica Química y Farmacia, Universidad Nacional de Tucumán, Ayacucho 471, 4000 San Miguel de Tucumán, Argentina
[b] Cátedra de Química General, Instituto de Química Inorgánica, Facultad de Bioquímica, Química y Farmacia, Universidad Nacional de Tucumán, Ayacucho 471, 4000 San Miguel de Tucumán, Tucumán, Argentina
[c] Instituto de Química, Pontificia Universidad Católica de Valparaíso, Valparaíso, Chile
[d] Departamento Disciplinario de Química, Facultad de Ciencias Naturales y Exactas, Universidad de Playa Ancha (UPLA), Valparaíso, Chile

HIGHLIGHTS

- The vibrational and electronic properties of dehydrofukinone were studied.
- Dehydrofukinone was investigated by using FTIR, FTRaman, NMR and UV spectroscopies.
- A complete vibrational analysis for dehydrofukinone was performed.
- The theoretical UV–visible spectrum has a good concordance with the experimental one.
- The calculated ^{1}H and ^{13}C chemicals shifts are in good agreement with the experimental ones.

GRAPHICAL ABSTRACT

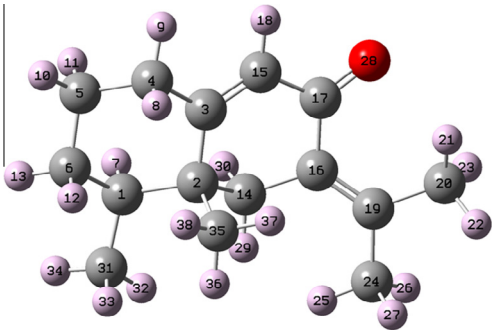

ARTICLE INFO

Article history:
Received 3 April 2013
Received in revised form 4 May 2013
Accepted 27 May 2013
Available online 11 June 2013

Keywords:
Dehydrofukinone
Vibrational spectra
Molecular structure
Force field
DFT calculations

ABSTRACT

The vibrational and electronic properties of 4β,5β-eremophil-7(11)9-dien-8-one, also known as dehydrofukinone (DHF), have been investigated by using experimental FT-IR, FT-Raman, NMR and UV spectra techniques and density functional theory (DFT) employing B3LYP exchange correlation with the 6-31G* and 6-311++G** basis sets. The calculated vibrational frequencies and the chemical shifts were successfully compared with the corresponding experimental values. The DFT calculations were combined with the Pulay's scaled quantum mechanical force field (SQMFF) methodology in order to perform a complete assignment of the observed bands in the vibrational spectra. The comparison of the theoretical ultraviolet–visible spectrum with the corresponding experimental demonstrates a good concordance. The natural bond orbital (NBO) study reveals for the isopropyliden and the two rings of DHF the characteristics of the electronic delocalization, while the corresponding topological properties of electronic charge density were analyzed by employing *Bader's* Atoms in the Molecules theory (AIM).

1. Introduction

Compounds containing rings in their structures are very interesting for research from different point of view because many of them present important biological activities [1–10]. The genus *Senecio*, is a largest and most complex genus in the family of the Asteraceae (Compositae) that have been extensively investigated for their secondary metabolites. Pyrrolizidine alkaloids, eremophilanolides and cacalolides are particularly characteristic for species of this genus [11]. Recently, the structure and the vibrational spectra of the antifungal 4-hydroxy-3-(3-methyl-2-butenyl) acetophe-

* Corresponding author. Tel.: +54 381 4247752; fax: +54 381 4248169.
E-mail address: sbrandan@fbqf.unt.edu.ar (S.A. Brandán).

0022-2860/$ - see front matter © 2013 Elsevier B.V. All rights reserved.
http://dx.doi.org/10.1016/j.molstruc.2013.05.067

none, isolated from *Senecio nutans* Sch. Bip. (Asteraceae), were studied [12] combining the infrared, Raman and NMR spectra with DFT calculations. The molecular structure of two mixed and closely related conformers of that acetophenone derivate were found in the solid with unequal occupancies by using X-ray diffraction methods and, then, a complete assignment of the vibrational spectra was performed by using a generalized valence force field (GVFF) [13,14]. Some compounds isolated from the genus *Senecio* and even crude extracts are known to possess antimicrobial activity, including antibacterial, antifungal, and antitubercular activities. In this work, we have studied the structural and vibrational properties of an eremophilane derived sesquiterpene ketone, the dehydrofukinone (DHF) that probably possesses interesting pharmacologic properties owing to the well known cytotoxic, antifungal and insect feeding deterrent activities of eremophilane sesquiterpenoids [15–19]. So far, molecular structure of DHF was not determined and there is no theoretical study concerning either geometry or vibrational spectra. DHF was described for the first time by Naya and coworkers [20] in *Arcticum lappa*, later as a constituent from *Cacalia hastata* [21], *Senecio humillimus* [22] and *Senecio aureus* [23]. First, dehydrofukinone was isolated from aerial parts of *Senecio viridis var. viridis* and then characterized by FTIR, FTRaman, NMR and UV–visible spectroscopies in the liquid state. Later, a theoretical study of DHF was performed in order to evaluate the theory best level and basis set to reproduce the experimental vibrational spectra and carry out its complete assignment. The normal mode calculations were accomplished by using a generalized valence force field (GVFF) together with the SQM methodology [14]. To complete the characterization of this interesting substance its solution phase ultraviolet–visible and NMR spectra are reported and discussed. The comparison of the theoretical ultraviolet–visible spectrum with the corresponding experimental one demonstrates a good concordance while the NMR spectra observed were successfully compared with the corresponding calculated chemical shifts at the two studied levels of theory. On the other hand, the characteristics of the electronic delocalization for isopropyliden group and the two rings of DHF and the topological properties of the electronic charge density for those rings were evaluated by means of NBO [24] and Atoms in Molecules (AIM) [25,26] studies.

2. Experimental methods

The DHF compound (oil) was isolated from aerial parts of *S. viridis var. viridis*. Leaves and flowers were extracted with methanol at room temperature for 3 days. After solvent evaporation, the residue was chromatographed on silica gel Merck 230–400 mesh using hexane–ethyl acetate mixtures of increasing polarity (97:3, 95:5, 93:7, 90:10, 87:13: 85:15 and 80:20). Fractions showing a single spot on TLC were reunited and the solvent evaporated to yield DHF as yellow oil. UV, EI–MS, ^{1}H and ^{13}C NMR spectra: were identical to the reported [14–17]. Purity: >99.98% by capillary gas chromatography using both flame ionization detector (FID) and selective mass detector.

The FT-IR spectrum in the region of 4000–400 cm^{-1} was recorded on a Fourier Transform Infrared (FT-IR) Perkin Elmer Spectrum RX spectrometer equipped with a DTGS (Deuterated TriGlycerine Sulfate) detector. The spectral resolution was 2 cm^{-1}, and 16 scans were performed. The spectrum was measured by putting one drop of the sample between KBr windows The Raman spectrum was recorded with a Renishaw Raman Microscope System RM2000 equipped with a diode laser providing a 634 nm line, a Leica microscope, an electrically cooled CCD (Charge Coupled Device) detector and a notch filter to eliminate elastic scattering. The spectrum was obtained by using a 50× objective. The laser power output was 2.0 mW, and the spectral resolution was 2 cm^{-1}.

Nuclear magnetic resonance (NMR) spectra were recorded on a Bruker 300 AVANCE spectrometer at 300 MHz for ^{1}H and 75 MHz for ^{13}C in $CDCl_3$ solutions containing 0.03 vol.% TMS as internal standard. GC–MS spectrum was recorded on a 5973 Hewlett–Packard selective mass detector coupled to a Hewlett Packard 6890 gas chromatograph equipped with a Perkin–Elmer Elite-5MS capillary column (5% phenyl methyl siloxane, length = 30 m, inner diameter = 0.25 mm, film thickness = 0.25 μm); ionization energy, 70 eV; carrier gas: helium at 1.0 mL/min. UV spectra were collected on a UV–visible 160 A Shimadzu spectrophotometer.

3. Computational details

The geometries of DHF were studied at the B3LYP/6-31G* and 6-311++G** theory levels. A stable conformation with C_1 symmetry was obtained for the compound using both calculations. The DHF's structure and the atoms labelling can be seen in Fig. 1. Natural population atomic (NPA) charges and bond orders for the DHF structure were also calculated at the same theory levels from the NBO calculation by using the NBO 3.1 program [26], as implemented in the Gaussian 03 package [27]. The topological analysis for the compound was performed by using the AIM2000 program package [25] while the MOLVIB program [28] was used to transform the resulting force fields to "natural" internal coordinates. The natural internal coordinates for DHF have been defined according to those reported in the literature [1–10,12,13], and are listed in Table S1 (Supporting material). The harmonic force field for the compound was evaluated at the B3LYP/6-31G* level using the procedure SQMFF [29]. Then, the complete assignment was performed with the resulting SQM only considering the potential energy distribution components (PED) ⩾ 10%. The nature of all the vibration normal modes was determinate by means of the GaussView program [30]. Ultraviolet–visible spectrum was predicted by using TD-DFT calculations at the B3LYP/6-31G* theory level. The calculated chemical shifts of the ^{1}H NMR and ^{13}C NMR for DHF were obtained by means the GIAO method [31] using the B3LYP/6-311++G** level of theory. The calculations have been performed using the geometries optimized for this level of theory and using TMS as reference.

4. Results and discussion

4.1. Geometry optimization

The potential energy and the dipole moment value are two important properties to describe the stability and the distributions

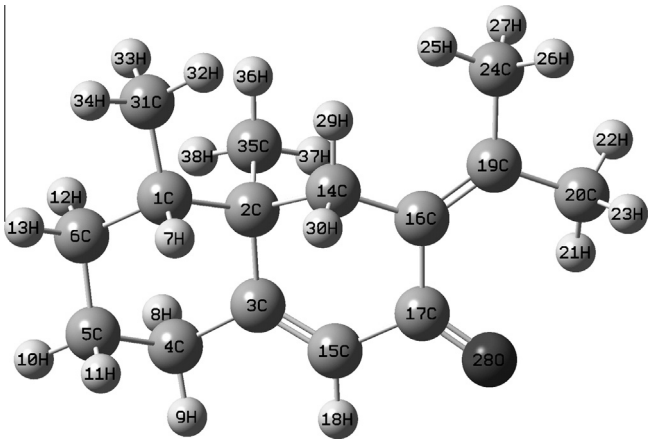

Fig. 1. Theoretical structure and atoms numbering of dehydrofukinone.

of charges on the atoms of a molecule. Here, both descriptors were calculated by using the B3LYP/6-31G* and B3LYP/6-311++G** calculations. Table S2 (Supporting material) shows the comparison of the total energies and the corresponding dipole moment values for the stable structure of DHF. It is important to note that the molecule of DHF has a certain polarity due to the presence of the carboxyl group. Thus, the highest dipole moment value and the more stable structure are obtained with the B3LYP/6-311++G** method, as expected because this level of calculation produce the better results due to its complete basis set. Table 1 shows a comparison of the calculated geometrical parameters for DHF by using the two methods of calculations, with the experimental values determined for the 6β,8β-dihydroxyeremophil-7(11)-en-8α, 12-olide by means of X-ray diffraction [32]. This eremophilane sesquiternoid has, as DHF, two six-membered rings that adopt chair conformations. The comparison by means of the root-mean-square deviation (RMSD) values shows that using both methods the bond lengths in DHF have a same correlation (0.070 Å) while the better values for the bond angles are observed using the 6-311++G** basis set (0.285°). The higher differences at these levels of calculation between both compounds are observed in the dihedral angles because the compared sesquiternoid has in its structure another five-member ring almost planar (0.016 Å). In DHF, the geometries obtained with both basis sets shows that the isopropyliden group and both rings are nearly coplanar, as they would be expected. These differences could probably justify that both sesquiternoids compounds exhibit different properties.

Table 1
Calculated geometrical parameters for the dehydrofukinone.

Parameter	[a]6-31G*	[a]6-311++G**	[b]Exp.
Bond length (Å)			
C1—C2	1.574	1.573	1.551(2)
C1—C31	1.537	1.536	1.531(3)
C1—C6	1.540	1.538	1.528(3)
C2—C3	1.530	1.528	1.558(2)
C2—C14	1.555	1.553	1.556(2)
C2—C35	1.549	1.549	1.538(2)
C3—C4	1.511	1.508	1.531(2)
C4—C5	1.536	1.535	1.517(3)
C5—C6	1.530	1.529	1.521(3)
C14—C16	1.516	1.514	1.323(2)
C15—C17	1.478	1.476	1.514(2)
C16—C17	1.495	1.494	1.497(2)
C16—C19	1.356	1.353	1.323(2)
C17—O28	1.231	1.227	1.394(2)
C3—C15	1.348	1.345	–
RMSD	0.070	0.070	
Bond angle (degrees)			
C1—C2—C35	111.91	111.88	111.07(15)
C2—C1—C31	114.10	114.07	114.13(15)
C1—C2—C14	108.44	108.45	110.06(14)
C1—C6—C5	111.91	111.93	113.11(16)
C6—C1—C31	110.05	110.17	109.68(16)
C16—C19—C24	123.82	123.64	–
C19—C16—C14	125.31	125.35	–
C16—C19—C20	124.06	124.18	–
C17—C16—C19	122.37	122.56	110.12(14)
O28—C17—C16	124.49	124.41	110.25(13)
C15—C3—C4	120.52	120.48	109.57(14)
C3—C2—C14	108.89	109.07	109.34(14)
RMSD	0.318	0.285	
Dihedral angles (degrees)			
O28—C17—C16—C19	24.20	27.72	–
C17—C15—C3—C2	−6.55	−6.33	−53.80(18)
C15—C3—C2—C35	100.41	102.01	169.56(15)
C15—C3—C2—C1	−137.21	−135.75	−68.34(17)
C35—C2—C1—C31	−54.29	−55.27	−58.1(2)
C14—C2—C1—C31	66.73	65.76	60.42(19)
C31—C1—C6—C5	−175.03	−174.92	−179.04(17)
C2—C14—C16—C19	126.87	125.37	−114.4(2)
C14—C16—C19—C24	0.20	0.58	−3.9(3)
RMSD	16.768	16.858	

[a] This work.
[b] From Ref [26].

4.2. NBO study

NBO calculations [24] were used to study the stability of DHF by using the atomic charges, bond orders and the second order perturbation energies. The natural atomic charges (NPA) for DHF by using 6-31G* and 6-311++G** basis sets are given in Table S3. The results show that, with both basis sets, the stability of DHF is associated respectively to the positive and negative high atomic charges values on the C17, C20, C24, O28, C31 and C35 atoms, in reference to the other ones. In relation to the bond orders, they are expressed by means of the Wiberg's indexes and are given in Table S4. Note that the bond orders values are slightly higher with the basis set of greater size, and for this reason, they are strongly dependent of the size of the basis set. Then, the values for the C2, C3, C16 and C19 atoms by using both basis sets are higher than the other ones. The double bond characters give explanation for the values observed in the bond orders of the C3, C16 and C19 atoms while the sp^3 hybridizing justify the corresponding bond order for the C2 atom. Probably, the same positions due to the chair conformation explain that the C16 atom has a similar bond order than the C19 atom.

On the other hand, the second-order perturbation energies $E^{(2)}$ (donor → acceptor) that involve the most important delocalization are presented in Table S5. The contributions of the stabilization energies to the $\Delta ET_{\sigma\rightarrow\sigma^*}$ charge transfers, due mainly to the present doubles bonds, are higher than the delocalization $\Delta ET_{LP\rightarrow\sigma^*}$ due to the free electron pairs of the oxygen atom. In addition, there are two other important delocalizations $\Delta ET_{\sigma^*\rightarrow\sigma^*}$ attributed to C═O double bond by using both basis sets. Thus, the total energy values clearly show two thinks, first, a highest stability of DHF by using the 6-31G* basis set and, second, that the stability is given by the ketonic function.

4.3. AIM analysis

The topological properties, such as the calculated charge electron density, (ρ) and the *Laplacian* values, $\nabla^2\rho(r)$ in the bond critical points (BCPs) and the ring critical points (RCPs) are shown in Table S6 and Fig. S1. Thus, for these critical points the values of $\rho(r)$ are between 0.05 and 0.3 a.u., the relationship, $|\lambda 1|/\lambda 3$ are <1 and the Laplacian of the electron density, $\nabla^2\rho(r)$ are positive and have values between 0.04 and 0.2 a.u., indicating that the interaction is dominated by the contraction of charge away from the interatomic surface toward each nucleus [4–10,12]. This analysis for both basis set, shows clearly the two expected RCPs, two BCPs, such as the H—H and O—H hydrogen bonds, which give rise to three new RCPs, as observed in Fig. S1. The results revels the high stability of this compound due to the hydrogen bonds and to the high values corresponding to RCP2 in relation to the other ones (See Fig. S1).

4.4. NMR analysis

Fig. S2 shows the ^{1}H NMR spectrum for DHF in $CDCl_3$, while Fig. S3 shows the corresponding ^{13}C NMR spectrum. Experimental and calculated chemical shifts for the ^{1}H and ^{13}C nuclei are compared in Tables S7 and S8 respectively. In general, the calculated shifts for the ^{13}C nuclei are higher than the corresponding experimental values. The calculated chemical shifts for the H nuclei show

a significant variation using 6-311++G** basis set (1.98 ppm) in relation to those calculated using 6-31G* basis set (0.41 ppm) and to the experimental values, while the chemical shifts for the carbon nuclei show higher RMSD values (9.461 and 5.390 ppm. respectively by using 6-31G* and 6-311++G** basis sets). The calculated ^{13}C chemical shifts show a good concordance for DHF by using the 6-311++G** basis set, as expected in accordance with other compounds [13,33–35]. Probably, the theoretical calculations do not correctly predict the hydrogen chemical shifts of the H nucleus belonging to the CH_3 groups, as observed in Table S7, due to the those groups are involved in intermolecular H-bonds, as observed by the AIM calculations (see Fig. S1). The NMR spectrum of fukinone [36] exhibits two singlets at 1.78 and 1.90 ppm for two methyls on a double bond, in this case, they are observed at 1.846 and 2.254 ppm. Table S8 shows that the calculated ^{13}C chemical shifts with the GIAO method using the 6-311++G** basis set are in accordance with the experimental values.

4.5. Vibrational analysis

The recorded infrared and Raman spectra for the compound can be seen in Figs. 2 and 3, respectively while the corresponding theoretical ones are observed in Fig. S4. The differences observed between both spectra are attributed to that in liquid phase the H bonds forces are important while the theoretical calculations are carry out in gas phase. The DHF structure have C_1 symmetry and 108 normal vibration modes, all active in the infrared and Raman spectra. The experimental and calculated wavenumbers for the expected normal vibration modes, the SQMFF based on the 6-31G* basis set, and the corresponding assignments are shown in Table 2. The assignment of the experimental bands to the normal modes of vibration was made taking into account the potential energy distribution (PED) and by using the B3LYP/6-31G* level. This method was employed because the used scale factors are only defined for this basis set [29]. The root mean square deviations (RMSD) obtained by comparing the experimental and calculated frequencies is 68.4 cm^{-1} for the 6-31G* basis set which was decreased until 15.1 cm^{-1} using the reported scale factors [29]. Notice that the groups of weak IR bands between 3500 and 3114 cm^{-1} indicate probably the existence of inter-molecular O—H···O bonds, in accordance with reported molecules [3–5,13,32–35,37,38] and with the results obtained by AIM analysis. Below, we discuss the assignment of the most important groups.

4.5.1. Bands assignments

4.5.1.1. CH modes. The DHF structure has two types of CH bonds, as observed in Fig. 1. On the one hand, the C15 atom has a sp^2 structure and for this reason, presents only a band in the IR spectrum at 3024 cm^{-1} which is associated with the C15—H18 stretching. On the other hand, the strong IR band at 2862 cm^{-1} can be easily assigned to the C1—H7 stretching modes because the C1 atom has a sp^3 structure, as observed in Table 2 and Fig. 1. The corresponding deformation modes were assigned to the IR band at 1344 cm^{-1} and to the Raman bands at 1331 and 1303 cm^{-1}. The remaining C—H modes were assigned as observed in Table 2.

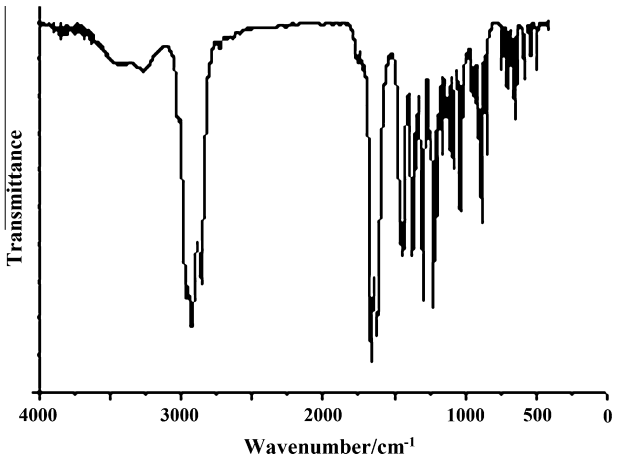

Fig. 2. Experimental infrared spectrum of dehydrofukinone.

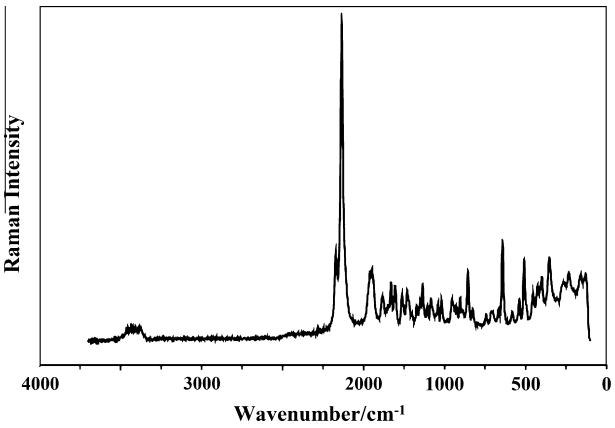

Fig. 3. Experimental Raman spectrum of dehydrofukinone.

4.5.1.2. CH_3 modes. The antisymmetric and symmetric stretching modes of methyl groups are calculated by SQM calculations as totally pure modes between 3056 and 2907 cm^{-1}, for this reason, those modes are assigned as observed in Table 2. The antisymmetric and symmetric CH_3 bending modes are predicted by calculations between 1474 and 1371 cm^{-1} according to the values reported for similar compounds [3,12,13,34]; hence, they were assigned in this region. Also, the rocking and twisting modes are clearly predicted in the expected regions for this group [3,12,13,34] and thus, they were assigned in those regions, as observed in Table 2.

4.5.1.3. CH_2 modes. The bands in the 2961–2862 cm^{-1} region can be easily assigned to CH_2 stretching modes, as observed in Table 2. The bending modes were assigned to the bands at 1461 and 1440 cm^{-1} while the wagging modes were associated with observed bands between 825 and 640 cm^{-1}. The expected rocking modes were assigned to the IR bands at 1247–1165 and to the Raman bands at 1263–1164 cm^{-1}, as indicated in Table 2. Finally, the twisting modes were in the 1380–1344 cm^{-1} region [2,3,5,7,12,13].

4.5.1.4. CO modes. The very strong band observed in the IR spectrum of the compound at 1662 cm^{-1} is easily assigned to the C=O stretching mode according to the values reported for similar compounds [1,3–6,12,13] and by the calculations. The weak IR band at 581 cm^{-1} is assigned to the C=O in plane deformation modes while the corresponding out-of-plane deformation mode is associated with the weak IR band at 741 cm^{-1}.

4.5.1.5. Skeletal modes. The description of the skeletal stretching modes can be seen in Table 2. The strong IR band at 1625 cm^{-1} and observed with very strong intensity in the Raman spectrum at 1635 cm^{-1}, in accordance with the predicted intensity, is assigned to the C=C stretching modes corresponding to the isopropyliden side chain and to the C=C corresponding to a ring. In the IR spectrum of fukinone [36] these modes are assigned to the bands at 1685 and 1625 cm^{-1}. According to the values previously

Table 2
Observed and calculated wavenumbers (cm^{-1}) and assignment for dehydrofukinone.

Mode	IR[a] solid	Raman[a]	Calculated[b]	SQM[c]	IR int.[d]	Raman act.[e]	Assignment[a]
1	3023 m		3188	3056	2.8	25.6	$\nu_{as}CH_3$ (C20)
2			3180	3048	14.3	121.8	ν_{as}(C15—H18)
3			3165	3034	32.1	39.8	$\nu_{as}CH_3$ (C24)
4			3138	3008	29.0	53.6	$\nu_{as}CH_2$ (C14)
5			3131	3001	26.1	39.8	$\nu_{as}CH_3$ (C35)
6			3128	2999	13.4	56.6	$\nu_{as}CH_3$ (C35)
7			3121	2992	25.7	15.7	$\nu_{as}CH_3$ (C31)
8			3111	2983	42.8	78.2	$\nu_{as}CH_3$ (C31)
9	2961 s		3089	2961	31.5	65.4	$\nu_{as}CH_2$ (C4)
10		2956 w	3083	2955	34.0	139.0	$\nu_{as}CH_2$ (C5)
11			3082	2955	51.5	165.4	$\nu_{as}CH_3$ (C20)
12	2929 s	2951 w	3076	2948	11.9	82.3	$\nu_{as}CH_3$ (C24)
13			3068	2941	58.7	145.4	$\nu_{as}CH_2$ (C6)
14			3060	2934	23.8	153.3	ν_sCH_3 (C35)
15			3052	2925	18.3	51.0	ν_sCH_3 (C31)
16			3040	2915	58.1	410.4	ν_sCH_3 (20)
17			3037	2911	30.2	58.5	ν_sCH_2 (C5)
18		2909 w	3033	2907	6.5	51.4	ν_sCH_3 (C24)
19			3028	2903	28.4	43.4	ν_sCH_2 (C6)
20	2874 sH	2873 w	3014	2889	35.7	87.4	ν_sCH_2 (C14)
21	2874 sh	2873 w	3012	2887	10.1	112.9	ν_sCH_2 (C4)
22	2862 s		3009	2877	5.9	26.7	ν(C1—H7)
23	1662 vs	1673 m	1740	1678	218.1	46.8	ν(C17—O28)
24	1625 s	1635 vs	1690	1629	42.5	222.6	ν(C15—C3)
25			1679	1616	102.9	74.2	ν(C16—C19)
26		1472 sh	1541	1474	0.3	5.4	$\delta_{as}CH_3$ (C31)
27			1536	1470	10.2	12.9	$\delta_{as}CH_3$ (C31)
28		1465 sh	1534	1467	5.6	5.7	δCH_2 (C6)
29	1461 s		1529	1463	0.14	8.0	$\delta_{as}CH_3$ (35)
30			1527	1460	2.1	31.7	δ_sCH_2 (C5)
31		1455 m	1523	1458	11.2	29.4	$\delta_{as}CH_3$ (C24)
32			1518	1453	2.4	8.9	$\delta_{as}CH_3$ (C24)
33			1516	1450	0.7	10.4	$\delta_{as}CH_3$ (C35)
34	1440 s		1511	1446	19.8	68.6	$\delta_{as}CH_3$ (C20)
35			1505	1439	2.1	7.4	δCH_2 (C14)
36			1503	1437	8.5	24.7	δCH_2 (C4)
37			1499	1434	5.5	17.4	$\delta_{as}CH_3$ (20)
38	1380 sh	1384 w	1447	1384	2.8	33.4	δ_sCH_3 (C24)
39			1443	1383	2.3	1.3	τwCH_2 (C6)
40			1437	1379	11.7	24.9	δ_sCH_3 (C20)
41			1431	1375	6.5	6.4	δ_sCH_3 (C31)
42			1411	1371	0.4	4.4	δ_sCH_3 (C35)
43	1370 s		1396	1370	4.3	4.3	τwCH_2 (C5)
44		1351 w	1390	1354	2.8	4.7	τwCH_2 (C4)
45	1344 m		1385	1349	5.4	12.1	ρ′CH(C1)
46			1371	1340	1.5	17.2	τwCH_2 (C14)
47		1331 m	1364	1334	8.7	2.1	βCH (C15)
48		1303 m	1349	1315	0.6	8.9	ρCH (C1)
49	1295 s		1327	1290	55.7	18.2	ν(C16—C17)
50		1263 m	1297	1259	0.3	15.6	ρCH_2 (C6)
51	1247 m		1288	1250	33.2	9.2	ρCH_2 (C14)
52	1225 s	1231 m	1253	1221	53.5	14.2	ρCH_2 (C5)
53		1202 w	1250	1218	17.0	4.9	$\nu_{as}CC_2$ (C19)
54	1193 s	1170 w	1226	1184	30.9	2.8	ν(C2—C14)
55	1165 m	1154 sh	1199	1160	15.2	8.6	ρCH_2 (C4)
56	1140 m	1136 m	1174	1140	0.6	11.6	ν(C1—C2)
57	1130 w		1168	1133	17.8	6.5	ρCH_3 (C24)
58	1120 m		1152	1114	7.9	1.7	ν(C6—C1)
59		1107 w	1150	1107	3.0	9.3	ν(C3—C4)
60	1102 m		1133	1088	8.9	4.4	τR^1 (A1)
61	1079 m	1082 w	1112	1085	13.8	0.8	$\rho' CH_3$ (C24)
62	1049 w		1100	1059	7.7	5.4	ν(C1—C31)
63	1036 s	1042 w	1073	1036	2.2	6.9	ρCH_3 (C35)
64	1015 m	1017 w	1057	1020	14.9	10.8	ν(C5—C6)
65	977 w	983 vw	1040	987	4.9	7.6	ν(C2—C35)
66	972 sh		1000	965	0.7	1.1	$\rho' CH_3$ (C20)
67	957 sh		993	958	4.7	3.2	$\rho' CH_3$ (C31)
68	951 m	954 w	979	951	0.4	3.0	ρCH_3 (C20)
69	925 m	929 w	968	930	3.4	8.2	ρCH_3 (C35)
70			959	922	1.1	3.6	ρCH_3 (C31)
71	907 sh		941	912	5.4	9.3	γ(C15—H18)
72	901 m	904 w	930	905	13.7	3.4	$\rho' CH_3$ (C35), βR_1 (A2)
73	884 s	888 sh	907	872	4.5	5.9	ν_sCC_2 (C19)
74	848 m	854 m	897	857	3.2	0.5	ν(C4—C5)

(*continued on next page*)

Table 2 (*continued*)

Mode	IR[a] solid	Raman[a]	Calculated[b]	SQM[c]	IR int.[d]	Raman act.[e]	Assignment[a]
75		825 w	870	820	2.7	5.1	wag CH_2 (C14)
76	826 sh		866	806	3.8	3.0	wag CH_2 (C6)
77	791 vw		838	783	0.2	3.3	wag CH_2 (C4)
78	741 w	746 w	757	736	3.2	3.3	γ(O28—C17)
79	702 w	708 w	718	695	3.1	3.1	ν(C14—C16)
80	666 m	667 w	705	682	5.8	1.8	ν(C2—C3)
81	640 m	640 s	674	652	3.4	1.8	wag CH_2 (C5)
82	611 sh		646	626	7.0	6.3	βR_2 (A2)
83	581 w	582 w	594	577	4.9	2.0	β(C17—O28)
84	556 sh	539 w	545	528	1.4	2.3	δC31C1C2
85	509 sh	510 m	514	503	0.6	4.6	γ(C19—C16)
86	495 w		503	489	2.7	0.9	βR_1 (A1)
87	455 vw	456 m	460	453	0.1	0.1	δC20C19C24, γ(C16—C19)
88	442 vw	426 m	426	417	0.1	1.8	βR_3 (A1)
89	430 vw	403 m	415	410	0.9	1.3	$\rho C19C_2$
90	413 vw	354 s	402	393	0.6	1.9	δC31C1C6, βR_3 (A2)
91			371	362	0.1	0.6	Butt
92			356	349	0.2	5.7	βR_2 (A1)
93			349	341	7.9	1.3	β(C16—C19)
94		327 sh	336	327	0.5	0.1	τR_2 (A1)
95		302 w	309	291	0.6	0.5	ρC2C35
96			283	278	0.7	2.0	ρ′C2C35
97		266 m	280	271	1.0	1.5	τR_3 (A2)
98		235 m	242	231	0.2	1.1	ρC2C35, τR_3 (A2), Butt
99			230	217	0.7	1.0	τCH_3 (C35), τCH_3 (C31)
100		206 sh	213	198	0.4	0.9	τR_3 (A1)
101			196	182	0.1	0.1	τCH_3 (C35)
102		160 m	174	168	1.1	2.2	τR_1 (A2)
103		126 m	133	119	0.4	0.5	τCH_3 (C24)
104			114	108	0.1	1.7	τCH_3 (C20), τR_2 (A1), τR_3 (A1)
105			104	97	0.8	0.2	τCCCC
106			99	91	0.2	0.5	τCH_3 (C20)
107			64	62	0.2	1.2	τCH_3 (C20), τR_2 (A2)
108			39	38	1.7	0.9	τR_2 (A2)

[a] This work.
[b] DFT B3LYP/6-31G*.
[c] From scaled quantum mechanics force field.
[d] Units are km mol^{-1}.
[e] Raman activities in $Å^4$ $(amu)^{-1}$.

reported for molecules with similar rings [37,38] and at the values obtained from our theoretical results, the deformations and torsions rings are associated with the IR bands observed between 1102 and 100 cm^{-1}, as observed in Table 2. The remaining skeletal modes were assigned as can be observed in Table 2.

5. Force field

The force constants expressed in terms of simple valence internal coordinates were calculated at the B3LYP/6-31G* and B3LYP/6-311++G** levels from the corresponding scaled force fields by using the MOLVIB program [28]. The force constants for DHF were estimated by using the SQM methodology [29] as was previously described in Section 3 and they are shown in Table 3. In general, the force constants have higher values with the B3LYP/6-31G* than the other calculation level indicating that the values are strongly dependent of the size of the basis set. The calculated *f*(νC=O) force constant value is in accordance with the values reported for similar molecules [1,3,4–6,12].

Table 3
Comparison of scaled internal force constants for dehydrofukinone.

Force constant	B3LYP/6-31G*[a]	B3LYP/6-311++G**[a]
f(νC=O)	11.115	10.750
f(νC=C)	8.464	8.271
f(νC—C)	4.030	3.963
f(νC—H)	4.840	4.779
f(νCH_2)	4.746	4.686
f(νCH_3)	4.874	4.796
f(δCH_2)	0.735	0.706
f(δCH_3)	0.553	0.529

Units are mdyn $Å^{-1}$ for stretching and stretching/stretching interaction and mdyn Å rad^{-2} for angle deformations.
[a] This work.

6. Ultraviolet–visible spectrum

The solution ethanol phase electronic spectrum of the substance is shown in Fig. 4 compared with the calculated spectrum at B3LYP/6-31G* level. Three bands located at 274, 249 and 208 nm can be experimentally observed, which should be assigned to the chromophores present in the molecule. The chromophoric system of DHF is a cross-conjugated system in which two overlapping α,β-unsaturated chromophoric groups are present. In this case, it should be expected that both systems give rise to transitions with reasonably large extinction coefficient. Although the estimated absorption for the less substituted (>C_3=C_{15}H—C_{17}=O) and for the more substituted (>C_{19}=C_{16}—C_{17}=O) α,β-unsaturated ketone systems of DHF using the Woodward-Fieser rules are λ_{max} 244 nm and λ_{max} 254 nm respectively, the observed absorption in ethanol appears at λ_{max} 249 nm, exactly at the middle of the estimated absorptions. It seems that because of the band nature of the spectra, the observed absorption correspond to the sum of both α,β-unsaturated ketone systems. The absorption at 280 nm could be assigned to the $\pi \rightarrow \pi^*$ transition corresponding to the entire crossed chromophoric system >C_3=C_{15}H—C_{17}=O—C_{16}=C_{19}<.

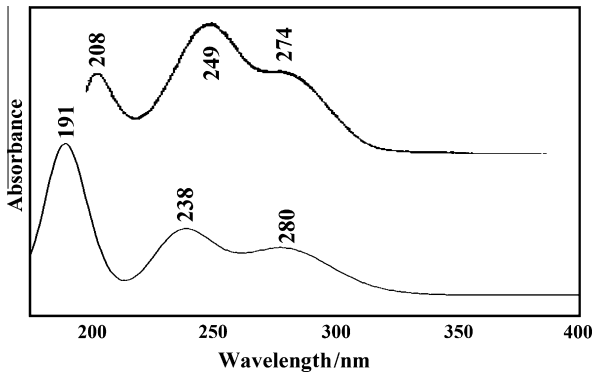

Fig. 4. Experimental in ethanol 96% (upper) and theoretical (bottom) ultraviolet–visible spectrum of dehydrofukinone.

Table 4
TD-DFT calculated visible absorption wavelengths (nm) and oscillator strengths (*f*) for dehydrofukinone.

Energy transition[a]	B3LYP6-31G*[a]		Exp. [a]	Assignment[a]
eV	λ (nm)	*f*	λ (nm)	
3.3258	372.80	0.0003		
4.4310	280.00	0.1458	274	$\pi \rightarrow \pi^*$ (cross-conjugated system)
5.2026	238.31	0.2065	249	$\pi \rightarrow \pi^*$ (β-unsaturated ketone)
5.4843	226.07	0.0025		
5.9649	207.86	0.0017		
6.5027	191.00	0.3587	208	$\pi \rightarrow \pi^*$ (C=C)

[a] This work.

The theoretical calculations predict one intense electronic transition at 6.5027 eV (191 nm) with an oscillator strength $f = 0.3587$.showing good agreement with the measured experimental data (208 nm) assigned to $\pi \rightarrow \pi^*$(C=C) transitions as shown in Table 4. The calculations also predict intense electronic transitions at 238 nm and 280 nm in good concordance with the experimental spectrum. The present assignments of the $\pi \rightarrow \pi^*$ transitions of DHF are in agreement with those of similar derivatives [39].

7. Conclusions

The compound was isolated from aerial parts of *S. viridis var. viridis* and characterized by IR, Raman, ultraviolet–visible and NMR spectroscopic techniques in the liquid state.

The theoretical molecular structures of dehydrofukinone were determined by using the B3LYP/6-31G* and B3LYP/6-311++G** methods. Both calculations levels show that the two six-membered rings adopt chair conformations and that the involved atoms in these rings present different atomic charges and bond orders values, as expected, because they have different chemical environments.

The stability of dehydrofukinone was studied by means of NBO and AIM investigations. The hyperconjugation between the electron donating groups shows larger energies values due to the ring containing the isopropyliden group and the ketonic function and revels that the $\Delta ET_{\sigma \rightarrow \sigma^*}$, $\Delta ET_{LP \rightarrow \sigma^*}$ and $\Delta ET_{\sigma^* \rightarrow \sigma^*}$ charge transfers stabilize the structure of dehydrofukinone. Additionally, the topological properties support the high stability of this compound due to the hydrogen bonds and to the high values corresponding to the six-membered linked to the isopropyliden group and the ketonic function.

A complete assignment of the 108 normal vibration modes for the compound was performed.

The SQM force fields and the scaled force constants by using the B3LYP/6-31G* and B3LYP/6-311++G** combinations were obtained.

The comparison of the theoretical ultraviolet–visible and NMR spectra with the corresponding experimental ones demonstrates a good concordance.

Acknowledgments

This work was supported with grants from CIUNT (Consejo de Investigaciones, Universidad Nacional de Tucumán) and CONICET (Consejo Nacional de Investigaciones Científicas y Técnicas, R. Argentina). The authors thank Prof. Tom Sundius for his permission to use MOLVIB.

Appendix A. Supplementary material

Supplementary data associated with this article can be found, in the online version, at http://dx.doi.org/10.1016/j.molstruc.2013.05.067.

References

[1] G.R. Argañaraz, E. Romano, J. Zinczuk, S.A. Brandán, J. Chem. Chem. Eng. 5 (2011) 747–758.
[2] C.D. Contreras, M. Montejo, J.J. Lopez Gonzalez, J. Zinczuk, S.A. Brandan, J. Raman Spectrosc. 42 (1) (2011) 108–116.
[3] E. Romano, A.B. Raschi, A. Benavente, S.A. Brandán, Spectrochim. Acta, Part A 84 (2011) 111–116.
[4] E. Romano, M.V. Castillo, J.L. Pergomet, J. Zinczuk, S.A. Brandán, J. Mol. Struct. 1018 (2012) 149–155.
[5] P. Leyton, J. Brunet, V. Silva, C. Paipa, M.V. Castillo, S.A. Brandán, Spectrochim. Acta, Part A: Mol. Biomol. Spectrosc. 88 (2012) 162–170.
[6] S.A. Brandán, F. Marquez Lopez, M. Montejo, J.J. Lopez Gonzalez, A. Ben Altabef, Spectrochim. Acta, Part A: Mol. Biomol. Spectrosc. 75 (2010) 1422–1434.
[7] E. Romano, N.A.J. Soria, R. Rudyk, S.A. Brandán, Mol. Simul. 38 (7) (2012) 561–566.
[8] A. Brizuela, E. Romano, A. Yurquina, S. Locatelli, S.A. Brandán, Spectrochim. Acta Part A 95 (2012) 399–406.
[9] E. Romano, N.A.J. Soria, R. Rudyk, S.A. Brandán, J. Asia Spectroscopy 17 (2013) 1–28.
[10] M.V. Castillo, E. Romano, A.B. Raschi, A. Yurquina, S.A. Brandán, Comput. Theor. Chem. 995 (2012) 43–48.
[11] E. Burgueño-Tapia, L.R. Hernández, A.Y. Reséndiz-Villalobos, P. Joseph-Nathan, Magn. Reson. Chem. 42 (2004) 887–892.
[12] E. Lizárraga, E. Romano, R.A. Rudyk, C.A.N. Catalán, S.A. Brandán, Spectrochim. Acta Part A: Mol. Biomol. Spectrosc. 97 (2012) 202–208.
[13] O.E. Piro, G.A. Echeverría, E. Lizarraga, E. Romano, C.A.N. Catalán, S.A. Brandán, Spectrochim. Acta Part A: Mol. Biomol. Spectrosc. 101 (2013) 196–203.
[14] P. Pulay, G. Fogarasi, F. Pang, E. Boggs, J. Am. Chem. Soc. 101 (10) (1979) 2550.
[15] J.-Q. Liu, M. Zhang, C.-F. Zhang, H-Y. Qi, A. Bashall, S.W.A. Bligh, Z.-T. Wang, Phytochemistry 69 (2008) 2231–2236.
[16] D.-Q. Fei, S.-G. Li, C.-M. Liu, G. Wu, K. Gao, J. Nat. Prod. 70 (2007) 241–245.
[17] D.-Q. Fei, Z.-C. Zhang, J.-J. Chen, K. Gao, Planta Med. 73 (12) (2007) 1292–1297.
[18] R.S. Burden, P.M. Rowell, J.A. Bailey, R.S.T. Loeffler, M.S. Kemp, C.A. Brown, Phytochemistry 24 (1985) 2191–2194.
[19] J. Nawrot, J. Harmatha, L. Novotny, Biochem. Syst. Ecol. 12 (1984) 99–101.
[20] K. Naya, K. Tsiju, U. Haku, Chem. Lett. (1972) 235.
[21] H. Hayasi, N. Hiroyuki, H. Mitsuhashi, Phytochemistry 12 (1973) 2931–2933.
[22] F. Bolmann, W. Kramp, H. Robinson, R.M. King, Phytochemistry 20 (1981) 1739–1740.
[23] R.J. Nachman, Phytochemistry 22 (3) (1983) 780–782.
[24] A.E. Reed, L.A. Curtis, F. Weinhold, Chem. Rev. 88 (6) (1988) 899–926; R.F.W. Bader, Atoms in Molecules, A Quantum Theory, Oxford University Press, Oxford, 1990, ISBN 0198558651.
[25] F. Biegler-Koning, J. Schonbohm, D. Bayles, J. Comput. Chem. 22 (2001) 545.
[26] E.D Glendening, J.K Badenhoop, A.D Reed, J.E Carpenter, F. Weinhold, NBO 3.1, Theoretical Chemistry Institute, University of Wisconsin, Madison, WI, 1996.
[27] M.J. Frisch, G.W. Trucks, H.B. Schlegel, G.E. Scuseria, M.A. Robb, J.R. Cheeseman, J.A. Montgomery, Jr., T. Vreven, K.N. Kudin, J.C. Burant, J.M. Millam, S.S. Iyengar, J. Tomasi, V. Barone, B. Mennucci, M. Cossi, G. Scalmani, N. Rega, G.A. Petersson, H. Nakatsuji, M. Hada, M. Ehara, K. Toyota, R. Fukuda, J. Hasegawa, M. Ishida, T. Nakajima, Y. Honda, O. Kitao, H. Nakai, M. Klene, C. Li, J.E. Knox, H.P. Hratchian, J.B. Cross, C. Adamo, J. Jaramillo, R. Gomperts, R.E. Stratmann, O. Yazyev, A.J. Austin, R. Cammi, C. Pomelli, J.W. Ochterski, P.Y. Ayala, K. Morokuma, G.A. Voth, P. Salvador, J.J. Dannenberg, V.G. Zakrzewski, S. Dapprich, A.D. Daniels, M.C. Strain, O. Farkas, D.K. Malick, A.D. Rabuck, K. Raghavachari, J.B. Foresman, J.V. Ortiz, Q. Cui, A.G. Baboul, S. Clifford, J. Cioslowski, B.B. Stefanov, G. Liu, A. Liashenko, P. Piskorz, I. Komaromi, R.L. Martin, D.J. Fox, T. Keith, M.A. Al-Laham, C.Y. Peng, A. Nanayakkara, M.

Challacombe, P.M.W. Gill, B. Johnson, W. Chen, M.W. Wong, C. Gonzalez, J.A. Pople, Gaussian Inc., Pittsburgh, PA, 2003.
[28] T. Sundius, Vib. Spectrosc. 29 (2002) 89–95.
[29] P. Pulay, G. Fogarasi, F. Pang, E. Boggs, J. Am. Chem. Soc. 105 (1983) 7037.
[30] A.B. Nielsen, A.J. Holder, Gauss View 3.0, User's Reference, Gaussian Inc., Pittsburgh, PA, 2000–2003.
[31] R. Ditchfield, Mol. Phys. 8 (1974) 397.
[32] Zhang, Fei, Acta Cryst. E67 (2011) o2957.
[33] A.E. Ledesma, J. Zinczuk, A. Ben Altabef, J.J. López-González, S.A. Brandán, J. Raman Spectrosc. 40 (8) (2009) 1004–1010.
[34] A.E. Ledesma, S.A. Brandán, J. Zinczuk, O.E. Piro, J.J. López González, A. Ben Altabef, J. Phys. Chem. Org. 21 (12) (2008) 1086.
[35] A.E. Ledesma, J. Zinczuk, J.J. Lopez Gonzalez, A. Ben Altabef, S.A. Brandan, J. Mol. Struct. 322 (2009) 924–926.
[36] K. Naya, I. Takagi, Y. Waguchi, Y. Asada, Tetrahedron 24 (1968) 5871–5879.
[37] L.C. Bichara, H.E. Lanús, S.A. Brandán, J. Chem. Chem. Eng. 5 (9) (2011).
[38] A.B. Brizuela, L.C. Bichara, E. Romano, A. Yurquina, S. Locatelli, S.A. Brandán, Carbohydr. Res. (2012).
[39] C.N Rao, Ultra-Violet and Visible Spectroscopy, Butterworth & Co., 1975.